Title

Stable Chelation of the Uranyl Ion by Acyclic Hexadentate Ligands: Potential Applications for 230U Targeted α-Therapy.

Journal

Inorganic Chemistry, 61(7)

Authors

Unnerstall, Ryan

Hasson, Abbie

Abou, Diane

et al.

Publication Date

2022-02-21

DOI

10.1021/acs.inorgchem.1c03972

Peer reviewed

HHS Public Access

Author manuscript

Inorg Chem. Author manuscript; available in PMC 2022 August 17.

Published in final edited form as:

Inorg Chem. 2022 February 21; 61(7): 3337–3350. doi:10.1021/acs.inorgchem.1c03972.

Stable Chelation of the Uranyl Ion by Acyclic Hexadentate Ligands: Potential Applications for ^{230}U Targeted Alpha Therapy

Joshua J. Woods[1,2,†], **Ryan Unnerstall**[3,4], **Abbie Hasson**[4,5], **Diane S. Abou**[3,4], **Valery Radchenko**[6,7], **Daniel L. J. Thorek**[3,4,5], **Justin J. Wilson**[1,*]

[1]Department of Chemistry and Chemical Biology, Cornell University, Ithaca, NY, 14853, USA.

[2]Robert F. Smith School for Chemical and Biomolecular Engineering, Cornell University, Ithaca, NY, 14853, USA.

[3]Department of Radiology, Washington University School of Medicine, St. Louis, MO, 63110, USA.

[4]Program in Quantitative Molecular Therapeutics, Washington University School of Medicine, St. Louis, MO, 63110, USA.

[5]Department of Biomedical Engineering, Washington University, St. Louis, MO, 63110, USA.

[6]Life Science Division, TRIUMF, Vancouver, BC Canada.

[7]Chemistry Department, University of British Columbia, Vancouver, BC, BC V6T 2A3, Canada.

Abstract

Uranium-230 is an α-emitting radionuclide with favorable properties for use in targeted alpha therapy (TAT), a type of nuclear medicine that harnesses α particles to eradicate cancer cells. To successfully implement this radionuclide for TAT, a bifunctional chelator that can stably bind uranium *in vivo* is required. To address this need, we investigated the acyclic ligands H_2dedpa, H_2CHXdedpa, H_2hox, and H_2CHXhox as uranium chelators. The stability revealing $\log\beta_{ML}$ values that are greater than 18 and 26 for the "pa" and "hox" chelators, respectively, signifying the resulting complexes to be exceedingly effective chelators for this ion. In addition, the UO_2^{2+} complexes were structurally characterized by NMR spectroscopy and X-ray crystallography. Crystallographic studies reveal that all six donor atoms of the four ligands span the equatorial plane of the UO_2^{2+} ion, giving rise to coordinatively saturated complexes that exclude solvent molecules. To further understand the enhanced thermodynamic stabilities of the "hox" chelators

[*]**Corresponding Author** jjw275@cornell.edu.

[†]Present Address: Chemical Sciences Division, Lawrence Berkeley National Laboratory, Berkeley, CA, 94720 USA.

Supporting Information

The Supporting Information is available free of charge at https://pubs.acs.org/doi/XXXXXX

Experimental details, spectroscopic and X-ray crystallographic characterization data, analytical titration data, computational studies (PDF).

Cartesian XYZ coordinates of DFT-optimized structures (.zip).

Accession Codes

CCDC 2087679–2087684 contain the supplementary crystallographic data for this paper. These data can be obtained free of charge via www.ccdc.cam.ac.uk/ data_request/cif, or by data_request@ccdc.cam.ac.uk, or by contacting The Cambridge Crystallographic Data Centre, 12 Union Road, Cambridge CB2 1EZ, UK; fax: +44 1223 336033

A provisional patent application has been filed on the use of these chelators for ^{230}U TAT.

over the “pa” chelators, density functional theory (DFT) calculations were employed. The use of the quantum theory of atoms in molecules (QTAIM) revealed that the extent of covalency between all four ligands and UO_2^{2+} was similar. Analysis of the DFT-computed ligand strain energy suggested that this factor was the major driving force for the higher thermodynamic stability of the “hox” ligands. To assess the suitability of these ligands for use with ^{230}U TAT in vivo, their kinetic stabilities were probed by challenging the UO_2^{2+} complexes with the bone model hydroxyapatite (HAP) and human plasma. All four complexes were >95% stable in human plasma for 14 d, whereas in the presence of HAP only the complexes of H_2CHXdedpa and H_2hox remained >80% intact over the same period. As a final validation of the suitability of these ligands for radiotherapy applications, the *in vivo* biodistribution of their UO_2^{2+} complexes were determined in mice in comparison to unchelated $[UO_2(NO_3)_2]$. In contrast to $[UO_2(NO_3)_2]$, which displays significant bone uptake, all four ligand complexes do not accumulate in the skeletal system, indicating that they remain stable *in vivo*. Collectively, these studies suggest that these equatorial-spanning ligands H_2dedpa, H_2CHXdedpa, H_2hox, and H_2CHXhox are highly promising candidates for use in ^{230}U TAT.

Graphical Abstract

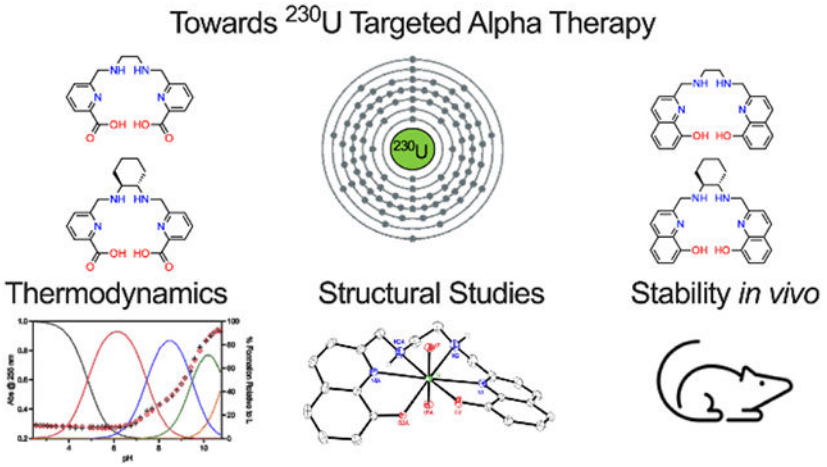

INTRODUCTION

Applied for the management of metastatic castration-resistant prostate cancer, radium-223 (^{223}Ra) is currently the only α-emitting radionuclide that is approved for clinical use in humans.[1] Administered as unchelated $[^{223}Ra]RaCl_2$, this radionuclide localizes to bone, where its high-energy α-particles effectively eradicate bone metastases. With this successful demonstration of the clinical value of α-emitting radionuclides for therapy, there has been significant interest in applying this therapeutic approach for targeting soft-tissue metastatic lesions as well as bone metastases. To accomplish this goal, an appropriate α-emitting radionuclide must be stably conjugated to high-affinity tumor-targeting moieties, such as antibodies, peptides, or small molecules using a bifunctional chelator. This concept, known as targeted alpha therapy (TAT), has prompted the investigation of other α-emitting radionuclides with more established conjugation chemistry.[1-5] Among the promising new candidates for this application is the radionuclide ^{230}U, which possesses a 20.8-day half-

life that is suitable for use with the long biological circulation time of antibody-based targeting vectors. This radionuclide produces five high-energy α-particles throughout its decay pathway to long-lived ^{210}Pb, which can cause lethal and localized damage to cancer cells (Scheme 1).[6,7] A potential advantage of ^{230}U with respect to other α-emitters is that its decay proceeds through a series of short-lived radionuclides, a feature that should minimize the translocation of these daughters from the target site after α recoil. Furthermore, promising production and purification strategies for ^{230}U have been reported,[7-11] suggesting that its widespread availability for sustaining preclinical and clinical studies may be achievable.

As noted above, the successful implementation of radiometals for TAT requires that they be conjugated to a biological targeting vector, such as an antibody or peptide, via a bifunctional chelator. In addition to being able to form a covalent bond with the targeting vector, an ideal bifunctional chelator must be able to stably chelate the desired radiometal with high thermodynamic stability and remain kinetically inert *in vivo* to prevent transchelation in the presence of endogenous ligands and macromolecules.[12] Despite the promising radiological properties of ^{230}U, it has not yet been evaluated for its therapeutic effects. The absence of such studies may partly be attributed to the lack of known chelators for stably binding uranium *in vivo*. The most stable form of uranium in aqueous solution is the uranyl ion (UO_2^{2+}) in which uranium exists formally in the 6+ oxidation state.[13-15] A unique feature of this ion is the presence of *trans*-oriented and strongly covalent U–oxo ($U–O_{yl}$) triple bonds.[16] Thus, as opposed to other radiometals under consideration for TAT that favor isotropic coordination spheres, appropriate chelators for ^{230}U must be able to accommodate the *trans*-dioxo ligands by binding to this metal center exclusively in the equatorial plane.

The chelation of UO_2^{2+} has been the subject of intense investigation over the last several decades primarily in the context of environmental and energy applications. For example, numerous studies have reported ligands for the extraction or sequestration of uranium from aqueous solution.[17-26] With respect to chelation of this ion in biological settings, there has also been extensive research efforts to develop ligands as decorporation agents for the removal of toxic concentrations of UO_2^{2+} from the body.[27-46] A feature shared by many of these ligands is the presence of hard oxygen donor atoms to maximally stabilize the highly oxophilic uranium center. To date, only one study has reported ligands specifically investigated for the implementation of ^{230}U in TAT. This report found that *para*-sulfonatocalix[6]- and calix[8]-arenes form complexes with UO_2^{2+} that display excellent thermodynamic stability, but poor kinetic stability in the presence of serum proteins.[38] As such, there remains a need for chelators that can stably bind UO_2^{2+} in biologically relevant environments.

In our search for stable uranium chelators, we sought ligands that selectively coordinate in the equatorial positions of the UO_2^{2+} ion. This search brought us to the family of acyclic ligands H_2dedpa, H_2CHXdedpa, H_2hox, and H_2CHXhox (Chart 1). These chelators are highly effective for the diagnostic radionuclides $^{67/68}$Ga, ^{64}Cu, and ^{111}In, forming complexes with excellent *in vivo* stability.[47-55] Given the high affinity of UO_2^{2+} for aminocarboxylate and 8-hydroxyquinoline (oxine) donors and its requirement for chelation in the equatorial plane, we hypothesized that these ligands would be an ideal match for

the stable chelation of this ion for nuclear medicine applications. Furthermore, because the ionic radius of U^{6+} (0.73 Å) is comparable to those of Ga^{3+} (0.62 Å), Cu^{2+} (0.73 Å), and In^{3+} (0.80 Å), ions that formed stable complexes with these ligands, we rationalized that the ligand cavity size would also be suitable for this application. In this work, we show them to be effective chelators for UO_2^{2+}, which form complexes with high thermodynamic stability and excellent kinetic inertness under biologically relevant conditions. Further, we investigated the biodistribution of the UO_2^{2+} complexes of these ligands to assess their *in vivo* stability. Ultimately, this work provides a better understanding of the requirements for stable chelators that can be employed to implement ^{230}U for TAT and highlights the value of this class of ligands for this application.

RESULTS AND DISCUSSION

Synthesis and Characterization of the Ligands.

The ligands H_2dedpa,[48,56,57] H_2CHXdedpa,[55,57] H_2hox[49,58] and H_2CHXhox[50] were synthesized by reductive amination reactions following slight modifications to previously reported procedures. The ligands were fully characterized by NMR spectroscopy, mass spectrometry, elemental analysis, and HPLC (Figures S1-S43). In addition, the solid-state structures of H_2CHXdedpa and H_2CHXhox were determined by X-ray crystallography (Figure S44). Relevant crystallographic parameters are given in Table S1 and a discussion of the structures is given in the Supporting Information (SI).

The protonation constants (pK_a) of these ligands have been previously reported in solutions with several different supporting electrolytes and ionic strengths.[48-50,55-58] Given that ionic strength and electrolyte can influence the obtained protonation constants of a ligand, we have replicated these studies in our preferred conditions of 0.1 M KCl using a combination of potentiometric (H_2dedpa and H_2CHXdedpa) or semi-batch spectrophotometric (H_2hox and H_2CHXhox) titration techniques (Table 1, Figures S45-S48). The obtained protonation constants from our measurements agree well with the previously reported values.

Solution UO_2^{2+} Complexation Studies.

With the ligand protonation constants in hand, we next evaluated the coordination of UO_2^{2+} by H_2dedpa, H_2CHXdedpa, H_2hox, and H_2CHXhox by measuring the thermodynamic stability constants ($\log\beta_{ML}$) of their UO_2^{2+} complexes using spectrophotometric titration techniques. Initial pH potentiometric experiments with UO_2^{2+} and H_2dedpa indicated that <5% of free UO_2^{2+} was present at our lowest electrode-calibrated pH value of 2.4 with the metal being entirely complexed at higher pH values. Thus, pH potentiometric titrations were unlikely to yield meaningful stability constants because these methods require a mixture of free and complexed metal ions over the pH range of the experiment. The poor aqueous solubility of the complexes at the relatively high (mM) concentrations required for these types of titrations further discounted their suitability for the determination of $\log\beta_{ML}$ values. To circumvent these challenges, we carried out spectrophotometric batch titrations following procedures similar to those previously reported for other metal complexation studies (Table 1, Figures S49-S53).[49,50,59,60] To support our aqueous equilibrium models, a Job's plot analysis of the UO_2^{2+} binding by the ligands was carried out, indicating that all of these

chelators exclusively formed 1:1 [(UO_2)L] complexes in solution (Figure S49). Additionally, the monoprotonated complex ($[MHL]^+$) could not be reasonably modeled based on the titration data over the pH ranges investigated for each ligand. A detailed discussion of the data-fitting process is included in the SI.

For H_2dedpa and H_2CHXdedpa, the logβ_{ML} values were found to be 18.1 and 18.8, respectively. The oxine ligands, H_2hox and H_2CHXhox, form significantly more stable complexes, as reflected by their large logβ_{ML} values of 26.4 and 26.7, respectively. Using an established density functional theory (DFT) method, we computed the stability constants and found the experimental values to be within ± 1 log unit of calculated values (Figure S54, Table S2). This excellent agreement confirms this computational approach to be a valuable tool for screening new ligands for UO_2^{2+} (Table 1).[61] Based on the ligand protonation constants and thermodynamic stability constants in Table 1, pH-dependent speciation diagrams for solutions containing UO_2^{2+} and each of the four ligands indicate that the major species present at pH 7.4 is the 1:1 ML complex for all four chelators (Figure 1).

The logβ_{ML} values reported in Table 1 are pH-independent absolute stability constants. Because these ligands can attain different protonation states, competition between H^+ and UO_2^{2+} binding will give rise to different pH-dependent conditional stability constants that make the direct comparison of logβ_{ML} values less useful. As an alternative means of comparing ligand affinity at physiological pH, we used pUO_2 values ($pUO_2 = -\log[UO_2^{2+}]_{free}$; $UO_2^{2+}{}_{free}$ = uncomplexed UO_2^{2+}), which is a measure of uncomplexed UO_2^{2+} that will be present at a given pH when the total ligand concentration is 10^{-5} M and the total UO_2^{2+} concentration is 10^{-6} M (Table 1).[46,62] Larger pUO_2 values are found for the ligands containing the cyclohexyl (CHX) backbone compared to their ethylenediamine (en) analogues, signifying stronger conditional binding at pH 7.4. The enhanced stability of the CHX ligands has previously been observed for their complexes of Ga^{3+}, Pb^{2+}, and Cd^{2+},[50,57,63] and has been attributed to the ability of the rigid CHX moiety to preorganize the ligand in a conformation that is favorable for metal chelation. The logβ_{ML} values of the oxine chelators are 2 log units greater than their picolinate counterparts, reflecting the higher affinity of 8-hydroxyquinoline for UO_2^{2+} over dipicolinic acid.[64,65] Notably, H_2hox and H_2CHXhox possess the highest pUO_2 values reported in the literature, indicating that they are highly suitable chelators for uranium.

In addition to forming stable complexes with the radionuclide of interest, a ligand must be able to rapidly bind to the metal ion in solution to minimize the extent of radioactive decay that occurs prior to administration of the radiolabeled pharmaceutical agent to the patient. Additionally, an ideal chelator should only require mild conditions (room temperature and physiological pH) for radiolabeling to avoid damaging the biological targeting vector. To assess the suitability of H_2dedpa, H_2CHXdedpa, H_2hox, and H_2CHXhox in this regard, we measured the second-order rate constants for their complexation of UO_2^{2+} in aqueous citrate (pH 5) or tris(hydroxymethyl)aminomethane (TRIS, pH 7.4) buffer at 25 °C using UV-vis spectroscopy (Figures S55-S58). Excess molar concentrations of these ligands were mixed with UO_2^{2+} to obtain pseudo first-order conditions.[60] The second-order rate constant for the

complexation reaction was then determined from the slope of a plot of the pseudo first-order rate constants versus ligand concentration.

The $[UO_2(L)]$ (L = $dedpa^{2-}$, $CHXdedpa^{2-}$, hox^{2-}, $CHXhox^{2-}$) complexes form rapidly in aqueous solution (Table 2). The second-order half-lives for the complexation reactions, calculated using concentrations of 10 μM for both L and UO_2^{2+}, are all under 4 min, signifying the expectation of fast reaction rates that will be highly favorable for radiotherapeutic applications. The complexation kinetics for H_2hox and H_2CHXhox showed a marked dependence on pH with significantly smaller second-order rate constants obtained at pH 5 compared to pH 7.4, which is most likely a consequence of the fact that the ligands are fully protonated at lower pH (Table 1). In contrast, the binding kinetics of the less basic H_2dedpa and H_2CHXdedpa ligands are relatively invariant to these two pH conditions. Comparison of the complexation kinetics of H_2CHXdedpa and H_2depda highlights the favorable effect of the preorganized CHX backbone towards metal chelation; H_2CHXdedpa can sequester free uranium twice as fast as its en-based counterpart. By contrast, the CHX group appears to have little influence on the complexation kinetics of H_2hox and H_2CHXhox. These chelators yield similar second-order rate constants for uranium complexation, suggesting that donor arm-binding, rather than secondary amine-binding, might be the rate-determining step for these ligands.

UO_2^{2+} Complex Structural Characterization.

The solution-state structures of the uranium complexes were explored using ^{1}H NMR spectroscopy. Spectra of $[UO_2(dedpa)]$ and $[UO_2(CHXdedpa)]$ were obtained in D_2O (Figure 2), whereas those for the significantly less water-soluble oxine complexes were acquired in DMSO-d_6 (Figure S59). The NMR spectra indicate the formation of compounds with C_2 symmetry, as evidenced by the chemical equivalency of the pendent donor groups. Furthermore, diastereotopic splitting of the methylene protons of the pendent arms further confirm complexation of UO_2^{2+}. Likewise, the methylene protons of the en backbone in H_2dedpa and H_2hox show diastereotopic splitting upon coordination (Figures 2a and S59a). By contrast, the protons corresponding to the CHX-backbone of the CHXdedpa and H_2CHXhox complexes do not undergo a change in the splitting pattern compared to the free ligands, presumably due to the rigidity of this group (Figures 2b and S59b). Collectively, the NMR spectra indicate that, in solution, the uranium center is being chelated in a symmetric manner with both pendent arms of all four ligands interacting equally with the metal.

The solid-state structures of the uranium complexes were examined using IR spectroscopy (Figures S60 and S61) and single-crystal X-ray diffraction (Figures 3 and 4). A detailed discussion of the IR spectra of the complexes is provided in the SI. X-ray diffraction quality crystals of $[UO_2(dedpa)]$ and $[UO_2(CHXdedpa)]$ were obtained by vapor diffusion of iPrOH into solutions of the complexes dissolved in mixtures of water and methanol and crystals of the hox complexes were obtained by slow vapor diffusion of Et_2O into methanolic solutions of the complexes at −20 °C over several weeks. Crystallographic parameters and relevant interatomic distances and angles are given in Tables 3 and S3. All four chelators feature hexadentate chelation of UO_2^{2+} with all the coordinating atoms lying in the equatorial plane, coordinatively saturating the metal center. Only three examples of hexadentate chelation of

UO_2^{2+} by acyclic ligands have been structurally characterized.[46,66,67] Overall, the structures agree well with their symmetric NMR spectra, and the characterization of these complexes as discrete 1:1 ML species is consistent with the Job's plot analyses.

The uranium center in each complex attains a distorted hexagonal bipyramidal geometry with the axial U–O_{yl} interatomic separations spanning 1.770(6)–1.799(3) Å among the four complexes. These distances are within the expected range for UO_2^{2+} complexes (Table 3). Within the structure of the H_2CHXhox complex, a hydrogen atom was located on the difference Fourier map, indicating that one of the 8-hydroxyquinoline arms is protonated to yield the complex $[UO_2(HCHXhox)]^+$ with the cationic charge balanced by an outer-sphere NO_3^- counteranion. As noted above, we were unable to reasonably model the monoprotonated MHL species from our titration data. The crystals of $[UO_2(HCHXhox)]^+$ were grown by vapor diffusion of diethyl ether into a methanolic solution containing $[UO_2(NO_3)_2]\cdot 6H_2O$, H_2CHXhox, and triethylamine at −20 °C over a period of several weeks, so it is unlikely that the speciation of the complex in aqueous solution is reflected by these conditions. In contrast to H_2CHXhox, the crystals of $[UO_2(hox)]$, which were obtained under similar conditions, revealed both oxygen atoms of the oxine arms to be deprotonated. Closer examination of the UO_2^{2+} moiety reveals that the O_{yl}–U–O_{yl} angle deviates significantly from linearity (169.89–172.84°) in each complex. A larger deviation is found in the complexes of the ligands containing the CHX backbone (Table 3). Given that this trend appears to depend on the ligand backbone rather than the nature of the donor atoms, we hypothesize that the origin of this O_{yl}–U–O_{yl} bending is due to steric interactions rather than electronic effects.[68]

With the exception of the protonated oxine arm in $[UO_2(HCHXhox)]^+$, the equatorial U–N and U–O interatomic distances are fairly consistent among the four complexes and exhibit maximum variations of only 0.05 Å within each bond type. In the structure of $[UO_2(HCHXhox)]^+$, the interatomic distance between the uranium center and the deprotonated oxine oxygen atom is considerably shorter (0.338 Å) than that of the protonated arm (Table 3). Collectively, these structural characteristics indicate that UO_2^{2+} is situated nearly symmetrically in the chelator binding pocket for all four ligands. The similarities of these solid-state uranium-donor atom interatomic distances do not reflect the significant differences between the thermodynamic affinities of these ligands for the UO_2^{2+}.

A series of metrics can be used to quantify the relative strain or distortion of a ligand upon chelation of UO_2^{2+} (Figure 5).[66,69] The first parameter, shown in Figure 5a, involves the equatorial bite angles of the chelator (σ_n) and the sum thereof ($\Sigma\sigma_n$). The angle between the amine nitrogen atoms in the backbone of the ligand (σ_3) can be considered the overall chelator bite angle.[70] The value of σ_3 is slightly larger (1–2°) for the ligands containing the CHX backbone as expected, based on the comparative rigidity of this group compared to en (Table 4). The bite angles of the picolinate and oxine moieties, σ_1 and σ_5, are relatively invariant. For a ligand that attains a perfectly planar conformation upon coordination, the value of $\Sigma\sigma_n$ will equal to 360°, whereas distortion of the equatorial plane, due to overcrowding, will lead to sum values that are greater than this value. All four complexes feature values of $\Sigma\sigma_n$ that are greater than 360° (Table 4), signifying a deviation from planarity caused by steric crowding about the uranium center. The structures

of [(UO_2)dedpa] and [UO_2(hox)] attain $\Sigma\sigma_n$ values that are close to 370°, whereas those containing the CHX ligands are more distorted from planarity as indicated by their larger $\Sigma\sigma_n$ values that hover near 375°. This deviation is further reflected in the large displacement of the donor atoms from the mean uranyl equatorial plane (Table S4). The oxygen donor atoms of the CHX ligands are displaced from this plane by more than 0.1 Å further than the en ligands. Thus, although the rigid CHX groups may enhance complexation kinetics and thermodynamic stability via preorganization effects, their lack of flexibility prevents the ligand from attaining a planar conformation when bound to UO_2^{2+}. The deviations of ligand planarity observed for these four complexes contrasts with several recently reported hexadentate pyrrole-based ligands, which can attain a nearly perfectly planar conformation ($\Sigma\sigma_n$ = 360.1–360.14°).[66]

Two other metrics used to characterize the ligand distortion (Figure 5b) include the angular deviation between the pendent arms (θ) and the angular deviation of the pendent arm from mean square plane defined by the equatorially coordinated donor atoms (φ). For a ligand that coordinates UO_2^{2+} in a planar fashion, such as bis(pyridyl-6-methyl-2-carboxylate)-ethylamine (dpaea),[71,72] θ and φ should be equal to 0°. High values of θ and φ indicate significant ruffling of the ligand upon chelation to UO_2^{2+}. The values of θ and φ for the four complexes are collected in Table 4. The large values of θ (>35°) and φ (>19°) found in all four complexes, indicate that these ligands are significantly ruffled, reflecting a similar degree of distortion that has been observed in several other uranium complexes of macrocyclic and acyclic ligands.[46,73,74] Collectively, these metric parameters $\Sigma\sigma_n$, θ, and φ indicate that none of the four ligands in this study can bind to UO_2^{2+} in a perfectly planar manner. However, the high stability constants afforded by these ligands suggest that this type of ideal coordination is not necessary for stable chelation of UO_2^{2+}.

Computational Studies.

The thermodynamic data described above indicate that the ligands containing 8-hydroxyquinoline pendent arms form more stable complexes with UO_2^{2+} than their picolinate-containing counterparts. Previous studies have established that the actinides can form covalent bonds in the equatorial plane that arise from overlap of the 5f and ligand-based orbitals.[74-82] As such, we hypothesized that the enhanced stability of H_2hox and H_2CHXhox compared to H_2dedpa and H_2CHXdedpa may be in part due to increased covalency in the equatorial interactions between the uranium center and the strongly donating oxine groups.[83] We investigated the nature of the metal-ligand interactions using Bader's Quantum Theory of Atoms in Molecules (QTAIM).[84] Within the QTAIM framework, the electron density (ρ) is divided into partitions by zero-flux surfaces and the bond path between two atoms is defined by the line of local maximum ρ between them. Along the bond path, the magnitude of ρ decreases and reaches its minimum at the intersection of the bond path and the zero-flux surface between the two atoms of interest, which is known as the bond critical point (BCP). The nature of the interatomic interactions between two atoms can be described using parameters at the BCP such as the electron density ρ_{BCP}, Laplacian of the electron density $\nabla^2\rho_{BCP}$, the Lagrangian kinetic G_{BCP}, potential V_{BCP}, and total energy H_{BCP} densities. It has been found that ρ_{BCP} and $\nabla^2\rho_{BCP}$ are inadequate for fully describing the bonding interactions of actinide complexes.[85,86]

As an alternative and more robust means of analysis, the ratio of potential and kinetic energies ($|V_{BCP}/G_{BCP}|$), and the normalized total energy density (H_{BCP}/ρ_{BCP}) are used to describe the nature of the interatomic interactions in actinide complexes.[87-93] These parameters have been benchmarked and validated as a means of assessing covalency within actinide-containing compounds.

The QTAIM parameters for the [UO_2(L)] complexes described here are compiled in Tables S5-S8 (Figure S62). As expected, QTAIM analysis finds six BCPs and bond paths between the uranium center and the six ligand-based oxygen and nitrogen donor atoms in all four complexes. At these BCPs, which reside closer to the ligand donor atoms than the uranium center, $\rho_{BCP} < 0.1$ e$^-$ Å^{-3} and $\nabla^2\rho_{BCP} > 0$ au, whereas $H_{BCP} < 0$ and $|V_{BCP}/G_{BCP}| > 1$. These values suggest that these interactions do possess a degree of covalency like other equatorial-spanning ligands found in related uranium compounds.[94-97] The degree of covalency can be analyzed by comparing the ratio of H_{BCP}/ρ_{BCP}.[88,89] As seen in Tables S5-S8, the values of H_{BCP}/ρ_{BCP} are largely invariant among the four complexes, indicating that all four ligands interact with UO_2^{2+} with a similar degree of covalency. Therefore, the significant differences in thermodynamic stability of the uranium complexes of these ligands cannot be solely explained through differences in metal-ligand covalency.

To explore alternative reasons for the significantly higher thermodynamic stabilities of the oxine complexes, we next calculated the ligand strain energies (ΔG_s) of chelation upon complexation of UO_2^{2+}. The strain energy is defined as the energy difference between the free ligand in its relaxed equilibrium conformation and that of the ligand in the conformation of the optimized metal complex (Figure S62).[98-100] This energy term reflects a degree of ligand preorganization and has been show to correlate with the metal-binding properties of polydentate ligands.[101-103] As seen in Table 5, ΔG_s decreases with increasing thermodynamic stability, indicating that conformational rigidity and preorganization of this ligand class plays an important role in their abilities to stably chelate the UO_2^{2+}. Somewhat unexpectedly, the effect of the rigid cyclohexyl group on the strain energy is less significant than that of the donor arms. For example, exchanging the picolinate donor arms for oxine donors decreases ΔG_s by approximately 30 kcal mol^{-1}, whereas introducing the cyclohexyl backbone but keeping the donor arms identical only decreases ΔG_s by 10 kcal mol^{-1}.

In Vitro UO_2^{2+} Complex Stability Studies.

Previous studies have shown that UO_2^{2+} binds to numerous biological species including albumin, transferrin, and carbonate with high affinity.[104-107] Accounting for the strengths of these interactions, a chelator with a binding constant of at least 10^{19} M^{-1} is required in order to stably chelate uranium *in vivo*.[104] According to this criterion, all four ligands investigated here are promising chelators for UO_2^{2+} for application in TAT. Although this prior speciation study provides a guideline for the required thermodynamic stability, kinetic inertness is another key criterion for the effective use of bifunctional chelator-radiometal complexes in nuclear medicine. To probe the kinetic stability of these uranium complexes, we first evaluated their ability to remain intact in the presence of hydroxyapatite (HAP), which is the main inorganic component of bone tissue. Uranium has a high affinity for this mineral, a fact that is reflected by its high uptake in bone upon accidental inhalation

or ingestion.[108] The deposition of high activity uranium isotopes in bone mineral causes both acute and chronic bone damage and cancer, events that must be avoided for the implementation of ^{230}U in TAT.

The four uranium complexes were incubated with 2000 equiv. of solid HAP in 0.1 M TRIS buffer at 37 °C. The amount of intact complex remaining in solution was analyzed by HPLC after 1 h, 24 h, 7 d, and 14 d (Figures 6 and S63). For comparison, $UO_2(NO_3)_2{\cdot}6H_2O$ was incubated under the same conditions, and the amount of remaining uranium in solution was monitored using the colorimetric indicator arsenazo III. As seen in Figure 6, $UO_2(NO_3)_2{\cdot}6H_2O$ is rapidly removed from solution by HAP in a matter of hours. Only 10% of the original uranium remains in solution after 12 h and by 120 h it is undetectable in solution. By contrast, [UO_2CHXdedpa] shows excellent kinetic stability under these conditions and remains >99% intact after 14 d. The other complexes are less kinetically stable under these conditions but remain >60% intact over the period investigated (Figure 6a). In the case of [UO_2(CHXhox)] only 15% of the initial complex remains in solution after 14 d. We note that this complex has a low solubility in water, especially at high ionic strength. Therefore, it is difficult to determine if the loss of complex from solution is a result of precipitation or dissociation of the complex in the presence of HAP. Although [UO_2(CHXdedpa)] does not possess the highest thermodynamic stability constant among the four complexes, it showed the greatest kinetic stability in the presence of HAP, underscoring the fact that thermodynamic affinity cannot always be used as a predictor of kinetic stability.

Because most TAT radiopharmaceutical agents are administered intravenously, we further investigated the kinetic stability of these complexes in human plasma. The four complexes were incubated in a 1:1 solution of TRIS buffer (0.1 M, pH 7.4) and human plasma at 37 °C, and the amount of intact complex was analyzed by HPLC (Figures 6 and S64). All four complexes display excellent kinetic stability in plasma and remain >98% intact after incubation for 14 d (Figure 6b). Previous studies have reported ligands capable of complexing UO_2^{2+} in blood, serum, or plasma.[29,31,44,109,110] However, none of these investigations examined the long-term (>10 d) stability of the complexes. This study is the first report to demonstrate the long-term stability of uranium complexes in human plasma, reflecting the potential value of these ligands for ^{230}U in TAT. The differing stability of the uranium complexes in the presence of HAP compared to plasma highlights how the kinetic stability of metal complexes is highly dependent on the local biological environment.

Biodistribution Studies.

In light of the promising kinetic stability of the uranium complexes in biologically relevant environments, we proceeded to evaluate their distribution *in vivo* in comparison to $UO_2(NO_3){\cdot}6H_2O$. Mice were treated with 4 mg/kg [$UO_2(NO_3)$]$\cdot6H_2O$, [UO_2(dedpa)], [UO_2(CHXdedpa)], or [UO_2(hox)] via intravenous injection, and the organs of interest, including the blood, heart, liver, lungs, spleen, kidney and bone (tibia), were excised at several timepoints for analysis of uranium content by inductively coupled plasma mass spectrometry (ICP-MS; Figure S65). The complex [UO_2(CHXhox)] was omitted from this study due to its poor aqueous solubility, which resulted in its precipitation in the circulatory system upon injection causing lethality. As observed in previous studies, with

the administration of $[UO_2(NO_3)]\cdot 6H_2O$ to mice results in a significant accumulation of uranium in bone (Figure 7a), as well as the spleen and kidneys.[111-115] Other bone-seeking heavy radionuclides, such as radium,[116,117] also localize to the spleen in small animals. In this study, renal retention of uranium was lower than expected based on related biodistribution experiments. Therefore, the biodistribution of this element may vary with the method and route of administration (acute versus chronic exposure and oral versus intravenous administration).[112,118]

In comparison to $[UO_2(NO_3)]\cdot 6H_2O$, the uranium complexes $[UO_2(dedpa)]$, $[UO_2(CHXdedpa)]$, and $[UO_2(hox)]$ were rapidly cleared from the blood with minimal uptake in the bone (Figure 7b-d). These data indicate that the complexes are being cleared rapidly, suggesting that the UO_2^{2+} is stably bound by these ligands *in vivo*. In addition, low but detectable values of uranium were found in the lung, liver and kidney upon treatment with $[UO_2(CHXdedpa)]$ and $[UO_2(dedpa)]$. Within mice treated with $[UO_2(hox)]$, significant accumulation of uranium in the lungs was observed. This aberrantly high lung uptake may arise from the precipitation of this compound upon intravenous injection because insoluble material in the blood will accumulate in the pulmonary capillaries. Notably, we observed no discernible redistribution of the uranium from organs of uptake to the bone at later time points. Although these results highlight the excellent kinetic stability of the uranium complexes *in vivo*, it should be noted that these experiments used ^{238}U as the source of uranium, which required substantially greater mass dose levels (4 mg/kg) of complex than would be required for a radiotracer study employing the much shorter-lived ^{230}U. As such, further verification of the distribution and stability of the ^{230}U complexes will be required.

CONCLUSIONS

In this report, we described the coordination chemistry of the chelators H_2dedpa, $H_2CHXdedpa$, H_2hox, and $H_2CHXhox$ with UO_2^{2+} as a means of assessing their potential use for ^{230}U TAT. These ligands are highly effective chelators for the diagnostic radionuclides ^{68}Ga, ^{64}Cu, and ^{111}In, forming stable octahedral coordination complexes. Through our X-ray crystallographic studies, we showed that they can also effectively span the equatorial plane of UO_2^{2+}, binding this ion with all six donors and providing a coordinatively saturated complex. Thermodynamic stability studies reveal that these ligands have high affinities for UO_2^{2+}. Notably, the pUO_2 values measured are the largest reported to date, indicating that these ligands are ideally suited for UO_2^{2+} chelation. Considering these high thermodynamic stabilities, it is noteworthy that the X-ray crystal structures reveal the ligands to deviate significantly from planarity upon UO_2^{2+} binding, suggesting that perfect planarity is not required for stable chelation of this ion. Although the more basic hox ligands are significantly more thermodynamically stable than the pa ligands, DFT and QTAIM calculations suggest a similar degree of covalency between the uranium center and the ligand donor atoms in each complex. The DFT-computed ligand strain energy, however, was found to be appreciably different for these two ligand classes, implicating this property to be an important factor in determining UO_2^{2+} stabilization. An unexpected result from the DFT strain energy calculations was that the presence of the cyclohexyl group had a smaller effect on this parameter than the picolinate and oxine donor arms. Thus, this

result suggests that an alternative approach to increase metal-ligand affinity is to focus on rigidifying the donor arms of acyclic ligands as well as the ligand backbone. Furthermore, our crystallographic analysis showed that there was little correlation of the planarity of the equatorial donor atoms with the stabilities of the complexes. Thus, it is feasible that hexadentate open-chain ligands with even greater affinity for UO_2^{2+} could be developed.

The kinetic stabilities of the uranium complexes of the ligands reported here under biologically relevant conditions were also investigated. The complexes are all sufficiently stable (>95%) in human plasma but differ in their labilities in the presence of HAP. Although H_2CHXdedpa does not possess the largest $\log\beta_{ML}$ among the four ligands tested, its uranium complex is the most stable to the HAP challenge, highlighting how thermodynamic affinities do not necessarily correlate with kinetic inertness. Lastly, biodistribution studies using murine models provided compelling evidence that the uranium complexes of H_2dedpa, H_2CHXdedpa, and H_2hox are stable *in vivo*, further validating their candidacy as chelators for targeted radiotherapy with ^{230}U.

In conclusion, this is the first study to describe the long-term stability of UO_2^{2+} coordination complexes in biological environments. Although chelators with high affinity for UO_2^{2+} have been reported, these ligands have primarily been employed as decorporation agents to remove this radionuclide from the body and demonstrations of their kinetic stabilities in biological systems are lacking. As such, this work will motivate continued efforts towards the successful implementation of ^{230}U in TAT. Ongoing work is focused on the development of targeted constructs employing these chelators for such applications.

Supplementary Material

Refer to Web version on PubMed Central for supplementary material.

ACKNOWLEDGEMENTS

The work reported in this publication was supported by the National Cancer Institute and National Institute of Biomedical Imaging and Bioengineering of the National Institutes of Health under Award Numbers NCI R01CA229893 (DLJT), R01CA201035 (DLJT), R01CA240711 (DLJT), NIBIB 1R01EB029259-01 (JJW). This research made use of the NMR Facility at Cornell University, which is supported, in part, by the U.S. National Science Foundation under award number CHE-1531632. TRIUMF receives funding via a contribution agreement with the National Research Council of Canada.

References

(1). Makvandi M; Dupis E; Engle JW; Nortier FM; Fassbender ME; Simon S; Birnbaum ER; Atcher RW; John KD; Rixe O; Norenberg JP Alpha-Emitters and Targeted Alpha Therapy in Oncology: From Basic Science to Clinical Investigations. Target. Oncol 2018, 13, 189–203. [PubMed: 29423595]

(2). Thiele NA; Wilson JJ Actinium-225 for Targeted α Therapy: Coordination Chemistry and Current Chelation Approaches. Cancer Biother. Radiopharm 2018, 33, 336–348. [PubMed: 29889562]

(3). Zalutsky M; Vaidyanathan G Astatine-211-Labeled Radiotherapeutics An Emerging Approach to Targeted Alpha-Particle Radiotherapy. Curr. Pharm. Des 2005, 6, 1433–1455.

(4). Yong K; Brechbiel MW Towards Translation of ^{212}Pb as a Clinical Therapeutic; Getting the Lead In! Dalton Trans. 2011, 40, 6068–6076. [PubMed: 21380408]

(5). Frantellizzi V; Cosma L; Brunotti G; Pani A; Spanu A; Nuvoli S; De Cristofaro F; Civitelli L; De Vincentis G Targeted Alpha Therapy with Thorium-227. Cancer Biother. Radiopharm 2020, 35, 437–445. [PubMed: 31967907]

(6). Alfassi ZB; Bonardi M; Groppi F; Menapace E A New Alpha-Emitter for Nuclear Medicine: ^{230}U. J. Radioanal. Nucl. Chem 2006, 270, 483–487.

(7). Morgenstern A; Apostolidis C; Bruchertseifer F; Capote R; Gouder T; Simonelli F; Sin M; Abbas K Cross-Sections of the Reaction ^{232}Th(p,3n)^{230}Pa for Production of ^{230}U for Targeted Alpha Therapy. Appl. Radiat. Isot 2008, 66, 1275–1280. [PubMed: 18374585]

(8). Morgenstern A; Lebeda O; Stursa J; Bruchertseifer F; Capote R; McGinley J; Rasmussen G; Sin M; Zielinska B; Apostolidis C Production of ^{230}U/^{226}Th for Targeted Alpha Therapy via Proton Irradiation of ^{231}Pa. Anal. Chem 2008, 80, 8763–8770. [PubMed: 18925748]

(9). Friend MT; Mastren T; Parker TG; Vermeulen CE; Brugh M; Birnbaum ER; Nortier FM; Fassbender ME Production of ^{230}Pa by Proton Irradiation of ^{232}Th at the LANL Isotope Production Facility: Precursor of ^{230}U for Targeted Alpha Therapy. Appl. Radiat. Isot 2020, 156, 108973. [PubMed: 31727509]

(10). Mastren T; Stein BW; Parker TG; Radchenko V; Copping R; Owens A; Wyant LE; Brugh M; Kozimor SA; Nortier FM; Birnbaum ER; John KD; Fassbender ME Separation of Protactinium Employing Sulfur-Based Extraction Chromatographic Resins. Anal. Chem 2018, 90, 7012–7017. [PubMed: 29757620]

(11). Hopkins PD; Mastren T; Florek J; Copping R; Brugh M; John KD; Nortier MF; Birnbaum ER; Kleitz F; Fassbender ME Synthesis and Radiometric Evaluation of Diglycolamide Functionalized Mesoporous Silica for the Chromatographic Separation of Actinides Th, Pa and U. Dalton Trans. 2018, 47, 5189–5195. [PubMed: 29528078]

(12). Price EW; Orvig C Matching Chelators to Radiometals for Radiopharmaceuticals. Chem. Soc. Rev 2014, 43, 260–290. [PubMed: 24173525]

(13). Endrizzi F; Rao L Chemical Speciation of Uranium(VI) in Marine Environments: Complexation of Calcium and Magnesium Ions with $[(UO_2)(CO_3)_3]^{4-}$ and the Effect on the Extraction of Uranium from Seawater. Chem. Eur. J 2014, 20, 14499–14506. [PubMed: 25213724]

(14). Van Horn JD; Huang H Uranium(VI) Bio-Coordination Chemistry from Biochemical, Solution and Protein Structural Data. Coord. Chem. Rev 2006, 250, 765–775.

(15). Cowie BE; Purkis JM; Austin J; Love JB; Arnold PL Thermal and Photochemical Reduction and Functionalization Chemistry of the Uranyl Dication, $[U^{VI}O_2]^{2+}$. Chem. Rev 2019, 119, 10595–10637. [PubMed: 31403292]

(16). Denning RG Electronic Structure and Bonding in Actinyl Ions and Their Analogs. J. Phys. Chem. A 2007, 111, 4125–4143. [PubMed: 17461564]

(17). Ivanov AS; Parker BF; Zhang Z; Aguila B; Sun Q; Ma S; Jansone-Popova S; Arnold J; Mayes RT; Dai S; Bryantsev VS; Rao L; Popovs I Siderophore-Inspired Chelator Hijacks Uranium from Aqueous Medium. Nat. Commun 2019, 10, 819. [PubMed: 30778071]

(18). Sather AC; Berryman OB; Rebek J Selective Recognition and Extraction of the Uranyl Ion. J. Am. Chem. Soc 2010, 132, 13572–13574. [PubMed: 20839791]

(19). Keener M; Hunt C; Carroll TG; Kampel V; Dobrovetsky R; Hayton TW; Ménard G Redox-Switchable Carboranes for Uranium Capture and Release. Nature 2020, 577, 652–655. [PubMed: 31969700]

(20). Marie C; Miguirditchian M; Guillaumont D; Tosseng A; Berthon C; Guilbaud P; Duvail M; Bisson J; Guillaneux D; Pipelier M; Dubreuil D Complexation of Lanthanides(III), Americium(III), and Uranium(VI) with Bitopic N,O Ligands: An Experimental and Theoretical Study. Inorg. Chem 2011, 50, 6557–6566. [PubMed: 21657800]

(21). Sun X; Tian G; Xu C; Rao L; Vukovic S; Kang SO; Hay BP Quantifying the Binding Strength of U(VI) with Phthalimidedioxime in Comparison with Glutarimidedioxime. Dalton Trans. 2014, 43, 551–557. [PubMed: 24126348]

(22). Bharara MS; Strawbridge K; Vilsek JZ; Bray TH; Gorden AEV Novel Dinuclear Uranyl Complexes with Asymmetric Schiff Base Ligands: Synthesis, Structural Characterization, Reactivity, and Extraction Studies. Inorg. Chem 2007, 46, 8309–8315. [PubMed: 17722915]

(23). Bauer A; Jäschke A; Schöne S; Barthen R; März J; Schmeide K; Patzschke M; Kersting B; Fahmy K; Oertel J; Brendler V; Stumpf T Uranium(VI) Complexes with a Calix[4]Arene-Based 8-Hydroxyquinoline Ligand: Thermodynamic and Structural Characterization Based on Calorimetry, Spectroscopy, and Liquid-Liquid Extraction. ChemistryOpen 2018, 7, 467–474. [PubMed: 29930893]

(24). Macor JA; Brown JL; Cross JN; Daly SR; Gaunt AJ; Girolami GS; Janicke MT; Kozimor SA; Neu MP; Olson AC; Reilly SD; Scott BL Coordination Chemistry of 2,2′-Biphenylenedithiophosphinate and Diphenyldithiophosphinate with U, Np, and Pu. Dalton Trans. 2015, 44, 18923–18936. [PubMed: 26466973]

(25). Dovrat G; Pevzner S; Berthon C; Lerner A; Maimon E; Vainer R; Karpasas M; Ben-Elyiahu Y; Moisy P; Bettelheim A; Zilbermann I Oligomers Intermediates in Between Two New Distinct Homonuclear Uranium(IV) DOTP Complexes**. Chem. Eur. J 2021, 27, 8264–8267. [PubMed: 33822408]

(26). Dovrat G; Illy MC; Berthon C; Lerner A; Mintz MH; Maimon E; Vainer R; Ben-Eliyahu Y; Moiseev Y; Moisy P; Bettelheim A; Zilbermann I On the Aqueous Chemistry of the U^{IV}–DOTA Complex. Chem. Eur. J 2020, 26, 3390–3403. [PubMed: 31943407]

(27). Overvoll PA; Lund W Complex Formation of Uranyl Ions with Polyaminopolycarboxylic Acids. Anal. Chim. Acta 1982, 143, 153–161.

(28). Deblonde GJP; Kelley MP; Su J; Batista ER; Yang P; Booth CH; Abergel RJ Spectroscopic and Computational Characterization of Diethylenetriaminepentaacetic Acid/Transplutonium Chelates: Evidencing Heterogeneity in the Heavy Actinide(III) Series. Angew. Chem. Int. Ed 2018, 57, 4521–4526.

(29). Wang X; Ji G; Shi C; Diwu J; Chen L; Gui D; Wan J; Silver MA; Wang J; Wang S Structural and Thermodynamic Stability of Uranyl-Deferiprone Complexes and the Removal Efficacy of U(VI) at the Cellular Level. Dalton Trans. 2018, 47, 8764–8770. [PubMed: 29916520]

(30). Durbin PW; Kullgren B; Ebbe SN; Xu J; Raymond KN Chelating Agents for Uranium(VI): 2. Efficacy and Toxicity of Tetradentate Catecholate and Hydroxypyridinonate Ligands in Mice. Health Phys. 2000, 78, 511–521. [PubMed: 10772024]

(31). Henge-Napoli MH; Archimbaud M; Ansoborlo E; Metivier H; Gourmelon P Efficacy of 3,4,3-LIHOPO for Reducing the Retention of Uranium in Rat after Acute Administration. Int. J. Radiat. Biol 1995, 68, 389–393. [PubMed: 7594963]

(32). Zhang Q; Jin B; Zheng T; Tang X; Guo Z; Peng R Hexadentate β-Dicarbonyl(Bis-Catecholamine) Ligands for Efficient Uranyl Cation Decorporation: Thermodynamic and Antioxidant Activity Studies. Inorg. Chem 2019, 58, 14626–14634. [PubMed: 31613591]

(33). Zhang Q; Jin B; Peng R; Lei S; Chu S Symmetrical 1,3-Dicarbonyl Biscatecholamide Ligands as Sequestering Agents for Uranyl Decorporation. Polyhedron 2015, 87, 417–423.

(34). Sawicki M; Lecerclé D; Grillon G; Le Gall B; Sérandour AL; Poncy JL; Bailly T; Burgada R; Lecouvey M; Challeix V; Leydier A; Pellet-Rostaing S; Ansoborlo E; Taran F Bisphosphonate Sequestering Agents. Synthesis and Preliminary Evaluation for in Vitro and in Vivo Uranium(VI) Chelation. Eur. J. Med. Chem 2008, 43, 2768–2777. [PubMed: 18313802]

(35). Ubios AM; Braun EM; Cabrini RL Lethality Due to Uranium Poisoning Is Prevented by Ethane-1-Hydroxy-1, l-Biphosphonate (EHBP). Health Phys. 1994, 66, 540–544. [PubMed: 8175360]

(36). Ye G; Roques J; Solari P-L; Den Auwer C; Jeanson A; Brandel J; Charbonnière LJ; Wu W; Simoni É Structural and Thermodynamics Studies on Polyaminophosphonate Ligands for Uranyl Decorporation. Inorg. Chem 2021, 60, 2149–2159. [PubMed: 33522798]

(37). Sonoda M; Nishida M; Ishii D; Yoshida I Super Uranophile, Water-Soluble Calixarenes: Their Metal Complexes, Stability Constants and Selective Reactivity to Uranyl Ion. Anal. Sci 1999, 15, 1207–1213.

(38). Montavon G; Repinc U; Apostolidis C; Bruchertseifer F; Abbas K; Morgenstern A Investigation of Para-Sulfonatocalix[n]Arenes [n = 6,8] as Potential Chelates for ^{230}U. Dalton Trans. 2010, 39, 1366–1374. [PubMed: 20104364]

(39). Sturzbecher-Hoehne M; Deblonde GJP; Abergel RJ Solution Thermodynamic Evaluation of Hydroxypyridinonate Chelators 3,4,3-LI(1,2-HOPO) and 5-LIO(Me-3,2-HOPO) for UO2(VI) and Th(IV) Decorporation. Radiochim. Acta 2013, 101, 359–366.

(40). Domingo JL; De La Torre A; Bellés M; Mayayo E; Llobet JM; Corbella J Comparative Effects of the Chelators Sodium 4,5-Dihydroxybenzene-1,3-Disulfonate (Tiron) and Diethylenetriaminepentaacetic Acid (DTPA) on Acute Uranium Nephrotoxicity in Rats. Toxicology 1997, 118, 49–59. [PubMed: 9074653]

(41). Bosque MA; Domingo JL; Llobet JM; Corbella J Effectiveness of Sodium 4,5-Dihydroxybenzene-1,3-Disulfonate (Tiron) in Protecting against Uranium-Induced Developmental Toxicity in Mice. Toxicology 1993, 79, 149–156. [PubMed: 8497868]

(42). Stradling GN; Gray SA; Moody JC; Ellender M Efficacy of Tiron for Enhancing the Excretion of Uranium from the Rat. Hum. Exp. Toxicol 1991, 10, 195–198. [PubMed: 1678949]

(43). Deblonde GJP; Lohrey TD; Booth CH; Carter KP; Parker BF; Larsen Å; Smeets R; Ryan OB; Cuthbertson AS; Abergel RJ Solution Thermodynamics and Kinetics of Metal Complexation with a Hydroxypyridinone Chelator Designed for Thorium-227 Targeted Alpha Therapy. Inorg. Chem 2018, 57, 14337–14346. [PubMed: 30372069]

(44). Wang X; Dai X; Shi C; Wan J; Silver MA; Zhang L; Chen L; Yi X; Chen B; Zhang D; Yang K; Diwu J; Wang J; Xu Y; Zhou R; Chai Z; Wang SA 3,2-Hydroxypyridinone-Based Decorporation Agent That Removes Uranium from Bones In Vivo. Nat. Commun 2019, 10, 2570. [PubMed: 31239437]

(45). Xu J; Raymond KN Uranyl Sequestering Agents: Correlation of Properties and Efficacy with Structure for UO_2^{2+} Complexes of Linear Tetradentate 1-Methyl-3-Hydroxy-2(1H)-Pyridinone Ligands. Inorg. Chem 1999, 38, 308–315.

(46). Szigethy G; Raymond KN Hexadentate Terephthalamide(Bis-Hydroxypyridinone) Ligands for Uranyl Chelation: Structural and Thermodynamic Consequences of Ligand Variation. J. Am. Chem. Soc 2011, 133, 7942–7956. [PubMed: 21542587]

(47). Boros E; Ferreira CL; Cawthray JF; Price EW; Patrick BO; Wester DW; Adam MJ; Orvig C Acyclic Chelate with Ideal Properties for ^{68}Ga PET Imaging Agent Elaboration. J. Am. Chem. Soc 2010, 132, 15726–15733. [PubMed: 20958034]

(48). Boros E; Cawthray JF; Ferreira CL; Patrick BO; Adam MJ; Orvig C Evaluation of the H_2Dedpa Scaffold and Its CRGDyK Conjugates for Labeling with ^{64}Cu. Inorg. Chem 2012, 51, 6279–6284. [PubMed: 22583103]

(49). Wang X; Jaraquemada-Peláez MDG; Cao Y; Pan J; Lin K-S; Patrick BO; Orvig C H_2Hox: Dual-Channel Oxine-Derived Acyclic Chelating Ligand for ^{68}Ga Radiopharmaceuticals. Inorg. Chem 2019, 58, 2275–2285. [PubMed: 29989801]

(50). Wang X; Jaraquemada-Peláez MDG; Cao Y; Ingham A; Rodríguez-Rodríguez C; Pan J; Wang Y; Saatchi K; Häfeli UO; Lin KS; Orvig C H2CHXhox: Rigid Cyclohexane-Reinforced Nonmacrocyclic Chelating Ligand for $[^{Nat/67/68}Ga]Ga^{3+}$. Inorg. Chem 2020, 59, 4895–4908. [PubMed: 32175726]

(51). Ramogida CF; Pan J; Ferreira CL; Patrick BO; Rebullar K; Yapp DTT; Lin KS; Adam MJ; Orvig C Nitroimidazole-Containing H_2Dedpa and H_2CHXdedpa Derivatives as Potential PET Imaging Agents of Hypoxia with ^{68}Ga. Inorg. Chem 2015, 54, 4953–4965. [PubMed: 25928800]

(52). Price EW; Zeglis BM; Cawthray JF; Ramogida CF; Ramos N; Lewis JS; Adam MJ; Orvig C H_4Octapa-Trastuzumab: Versatile Acyclic Chelate System for ^{111}In and ^{177}Lu Imaging and Therapy. J. Am. Chem. Soc 2013, 135, 12707–12721. [PubMed: 23901833]

(53). Boros E; Ferreira CL; Yapp DTT; Gill RK; Price EW; Adam MJ; Orvig C RGD Conjugates of the H_2dedpa Scaffold: Synthesis, Labeling and Imaging with ^{68}Ga. Nucl. Med. Biol 2012, 39, 785–794. [PubMed: 22381779]

(54). Ramogida CF; Boros E; Patrick BO; Zeisler SK; Kumlin J; Adam MJ; Schaffer P; Orvig C Evaluation of H_2CHXdedpa, H_2dedpa and H_2CHXdedpa-N,N′-Propyl-2-NI Ligands for ^{64}Cu(II) Radiopharmaceuticals. Dalton Trans. 2016, 45, 13082–13090. [PubMed: 27161975]

(55). Ramogida CF; Cawthray JF; Boros E; Ferreira CL; Patrick BO; Adam MJ; Orvig C H_2CHXdedpa and H_4CHXoctapa-Chiral Acyclic Chelating Ligands for$^{67/68}$Ga and ^{111}In Radiopharmaceuticals. Inorg. Chem 2015, 54, 2017–2031. [PubMed: 25621728]

(56). Platas-Iglesias C; Mato-Iglesias M; Djanashvili K; Muller RN; Vander Elst L; Peters JA; De Blas A; Rodríguez-Blas T Lanthanide Chelates Containing Pyridine Units with Potential Application as Contrast Agents in Magnetic Resonance Imaging. Chem. Eur. J 2004, 10, 3579–3590. [PubMed: 15252806]

(57). Ferreirós-Martínez R; Esteban-Gómez D; Platas-Iglesias C; de Blas A; Rodríguez-Blas T Zn(II), Cd(II) and Pb(II) Complexation with Pyridinecarboxylate Containing Ligands. Dalton Trans. 2008, 5754–5765. [PubMed: 18941663]

(58). Hata T; Uno T Studies on New Derivatives of 8-Quinolinol as Chelating Agents. I. Syntheses, Coloration Reaction with Metal Ions and Acid Dissociation Constants of Some Azomethine and Aminomethyl Derivatives. Bull. Chem. Soc. Jpn 1972, 45, 477–481.

(59). Hu A; Keresztes I; MacMillan SN; Yang Y; Ding E; Zipfel WR; Distasio RA; Babich JW; Wilson JJ Oxyaapa: A Picolinate-Based Ligand with Five Oxygen Donors That Strongly Chelates Lanthanides. Inorg. Chem 2020, 59, 5116–5132. [PubMed: 32216281]

(60). Pham TA; Xu J; Raymond KN A Macrocyclic Chelator with Unprecedented Th^{4+} Affinity. J. Am. Chem. Soc 2014, 136, 9106–9115. [PubMed: 24870296]

(61). Vukovic S; Hay BP; Bryantsev VS Predicting Stability Constants for Uranyl Complexes Using Density Functional Theory. Inorg. Chem 2015, 54, 3995–4001. [PubMed: 25835578]

(62). Harris WR; Carrano CJ; Raymond KN Coordination Chemistry of Microbial Iron Transport Compounds. 16. Isolation, Characterization, and Formation Constants of Ferric Aerobactin. J. Am. Chem. Soc 1979, 101, 2722–2727.

(63). Ramogida CF; Cawthray JF; Boros E; Ferreira CL; Patrick BO; Adam MJ; Orvig C H_2*CHX*dedpa and H_4*CHX*octapa –Chiral Acyclic Chelating Ligands for $^{67/68}$Ga and ^{111}In Radiopharmaceuticals. Inorg. Chem 2015, 54, 2017–2031. [PubMed: 25621728]

(64). Ünak P; Özdemir D; Ünak T Stability Constants of Uranium(VI) and Thorium(IV) Complexes Formed with 8-Hydroxyquinoline and Its 5-Sulfonic Acid Derivative. J. Radioanal. Nucl. Chem. Lett 1994, 186, 325–332.

(65). Ahmed IT; El-Roudi OM; Boraei AAA; Ibrahim SA Equilibrium Studies of the Ternary Complex Systems M^{N+} + Dipicolinic Acid + N-(2-Acetamido)Iminodiacetic Acid or Amino Acids. J. Chem. Eng. Data 1996, 41, 386–390.

(66). Mayhugh JT; Niklas JE; Forbes MG; Gorden JD; Gorden AEV Pyrrophens: Pyrrole-Based Hexadentate Ligands Tailor-Made for Uranyl (UO_2^{2+}) Coordination and Molecular Recognition. Inorg. Chem 2020, 59, 9560–9568. [PubMed: 32590898]

(67). Noufele CN; Pham CT; Hagenbach A; Abram U Uranyl Complexes with Aroylbis(N, N-Dialkylthioureas). Inorg. Chem 2018, 57, 12255–12269. [PubMed: 30222328]

(68). Hayton TW Understanding the Origins of Oyl-U-Oyl Bending in the Uranyl (UO_2^{2+}) Ion. Dalton Trans. 2018, 47, 1003–1009. [PubMed: 29292425]

(69). Szigethy G; Raymond KN The Influence of Linker Geometry in Bis(3-Hydroxy-N-Methyl-Pyridin-2-One) Ligands on Solution Phase Uranyl Affinity. Chem. Eur. J 2011, 17, 1818–1827. [PubMed: 21274933]

(70). Szigethy G; Raymond KN Influence of Linker Geometry on Uranyl Complexation by Rigidly Linked Bis(3-Hydroxy-N-Methyl-Pyridin-2-One). Inorg. Chem 2010, 49, 6755–6765. [PubMed: 20575583]

(71). Faizova R; Fadaei-Tirani F; Bernier-Latmani R; Mazzanti M Ligand-Supported Facile Conversion of Uranyl(VI) into Uranium(IV) in Organic and Aqueous Media. Angew. Chem. Int. Ed 2020, 59, 6756–6759.

(72). Faizova R; Scopelliti R; Chauvin AS; Mazzanti M Synthesis and Characterization of a Water Stable Uranyl(V) Complex. J. Am. Chem. Soc. 2018, 140, 13554–13557. [PubMed: 30289696]

(73). Brewster Ii JT; He Q; Anguera G; Moore MD; Ke X-S; Lynch VM; Sessler JL Synthesis and Characterization of a Dipyriamethyrin–Uranyl Complex. Chem. Commun 2017, 53, 4981–4984.

(74). Brewster JT; Mangel DN; Gaunt AJ; Saunders DP; Zafar H; Lynch VM; Boreen MA; Garner ME; Goodwin CAP; Settineri NS; Arnold J; Sessler JL In-Plane Thorium(IV), Uranium(IV), and Neptunium(IV) Expanded Porphyrin Complexes. J. Am. Chem. Soc 2019, 141, 17867–17874. [PubMed: 31609114]

(75). Tian G; Teat SJ; Zhang Z; Rao L Sequestering Uranium from Seawater: Binding Strength and Modes of Uranyl Complexes with Glutarimidedioxime. Dalton Trans. 2012, 41, 11579–11586. [PubMed: 22801978]

(76). Vitova T; Pidchenko I; Fellhauer D; Bagus PS; Joly Y; Pruessmann T; Bahl S; Gonzalez-Robles E; Rothe J; Altmaier M; Denecke MA; Geckeis H The Role of the 5f Valence Orbitals of Early Actinides in Chemical Bonding. Nat. Commun 2017, 8, 16053. [PubMed: 28681848]

(77). King RB Some Aspects of Structure and Bonding in Binary and Ternary Uranium(VI) Oxides. Chem. Mater 2002, 14, 3628–3635.

(78). Di Pietro P; Kerridge A Assessing Covalency in Equatorial U-N Bonds: Density Based Measures of Bonding in BTP and Isoamethyrin Complexes of Uranyl. Phys. Chem. Chem. Phys 2016, 18, 16830–16839. [PubMed: 27279271]

(79). Minasian SG; Keith JM; Batista ER; Boland KS; Clark DL; Conradson SD; Kozimor SA; Martin RL; Schwarz DE; Shuh DK; Wagner GL; Wilkerson MP; Wolfsberg LE; Yang P Determining Relative f and d Orbital Contributions to M-Cl Covalency in MCl_6^{2-} (M = Ti, Zr, Hf, U) and $UOCl_5^-$ Using Cl K-Edge X-Ray Absorption Spectroscopy and Time-Dependent Density Functional Theory. J. Am. Chem. Soc 2012, 134, 5586–5597. [PubMed: 22404133]

(80). Klamm BE; Windorff CJ; Celis-Barros C; Marsh ML; Albrecht-Schmitt TE Synthesis, Spectroscopy, and Theoretical Details of Uranyl Schiff-Base Coordination Complexes. Inorg. Chem 2020, 59, 23–31. [PubMed: 31009208]

(81). Tassell MJ; Kaltsoyannis N Covalency in $AnCp_4$ (An = Th–Cm): A Comparison of Molecular Orbital, Natural Population and Atoms-in-Molecules Analyses. Dalton Trans. 2010, 39, 6719–6725. [PubMed: 20631951]

(82). Kelley MP; Deblonde GJP; Su J; Booth CH; Abergel RJ; Batista ER; Yang P Bond Covalency and Oxidation State of Actinide Ions Complexed with Therapeutic Chelating Agent 3,4,3-LI(1,2-HOPO). Inorg. Chem 2018, 57, 5352–5363. [PubMed: 29624372]

(83). Fiszbein DJ; Brown V; Thiele NA; Woods JJ; Wharton L; Macmillan SN; Radchenko V; Ramogida CF; Wilson JJ Tuning the Kinetic Inertness of Bi3+Complexes: The Impact of Donor Atoms on Diaza-18-Crown-6 Ligands as Chelators for 213Bi Targeted Alpha Therapy. Inorg. Chem 2021, 60, 9199–9211. [PubMed: 34102841]

(84). Bader RFW Atoms in Molecules. Acc. Chem. Res 1985, 18, 9–15.

(85). Mountain ARE; Kaltsoyannis N Do QTAIM Metrics Correlate with the Strength of Heavy Element-Ligand Bonds? Dalton Trans. 2013, 42, 13477–13486. [PubMed: 23897486]

(86). Kerridge A Quantification of F-Element Covalency through Analysis of the Electron Density: Insights from Simulation. Chem. Commun 2017, 53, 6685–6695.

(87). Dan D; Celis-Barros C; White FD; Sperling JM; Albrecht-Schmitt TE Origin of Selectivity of a Triazinyl Ligand for Americium(III) over Neodymium(III). Chem. Eur. J 2019, 25, 3248–3252. [PubMed: 30716170]

(88). White FD; Gaiser AN; Warzecha EJ; Sperling JM; Celis-Barros C; Salpage SR; Zhou Y; Dilbeck T; Bretton AJ; Meeker DS; Hanson KG; Albrecht-Schmitt TE Examination of Structure and Bonding in 10-Coordinate Europium and Americium Terpyridyl Complexes. Inorg. Chem 2018, 57, 12969–12975. [PubMed: 30265525]

(89). Windorff CJ; Celis-Barros C; Sperling JM; McKinnon NC; Albrecht-Schmitt TE Probing a Variation of the Inverse-Trans-Influence in Americium and Lanthanide Tribromide Tris(Tricyclohexylphosphine Oxide) Complexes. Chem. Sci 2020, 11, 2770–2782. [PubMed: 34084337]

(90). Mansell SM; Kaltsoyannis N; Arnold PL Small Molecule Activation by Uranium Tris(Aryloxides): Experimental and Computational Studies of Binding of N_2, Coupling of CO, and Deoxygenation Insertion of CO_2 under Ambient Conditions. J. Am. Chem. Soc 2011, 133, 9036–9051. [PubMed: 21591662]

(91). Berryman VEJ; Shephard JJ; Ochiai T; Price AN; Arnold PL; Parsons S; Kaltsoyannis N Quantum Chemical Topology and Natural Bond Orbital Analysis of M-O Covalency in $M(OC_6H_5)_4$ (M = Ti, Zr, Hf, Ce, Th, Pa, U, Np). Phys. Chem. Chem. Phys 2020, 22, 16804–16812. [PubMed: 32662500]

(92). Berryman VEJ; Whalley ZJ; Shephard JJ; Ochiai T; Price AN; Arnold PL; Parsons S; Kaltsoyannis N Computational Analysis of M–O Covalency in $M(OC_6H_5)_4$ (M = Ti, Zr, Hf, Ce, Th, U). Dalton Trans. 2019, 48, 2939–2947. [PubMed: 30720806]

(93). Arnold PL; Prescimone A; Farnaby JH; Mansell SM; Parsons S; Kaltsoyannis N Characterizing Pressure-Induced Uranium C–H Agostic Bonds. Angew. Chem. Int. Ed 2015, 54, 6735–6739.

(94). Vallet V; Wahlgren U; Grenthe I Probing the Nature of Chemical Bonding in Uranyl(VI) Complexes with Quantum Chemical Methods. J. Phys. Chem. A 2012, 116, 12373–12380. [PubMed: 23151258]

(95). Denning RG; Green JC; Hutchings TE; Dallera C; Tagliaferri A; Giarda K; Brookes NB; Braicovich L Covalency in the Uranyl Ion: A Polarized x-Ray Spectroscopic Study. J. Chem. Phys 2002, 117, 8008–8020.

(96). Pace KA; Klepov VV; Berseneva AA; Loye H Covalency in Actinide Compounds. Chem. Eur. J 2021, 27, 5835–5841. [PubMed: 33283323]

(97). Kelley MP; Su J; Urban M; Luckey M; Batista ER; Yang P; Shafer JC On the Origin of Covalent Bonding in Heavy Actinides. J. Am. Chem. Soc 2017, 139, 9901–9908. [PubMed: 28657317]

(98). Wilson JJ; Ferrier M; Radchenko V; Maassen JR; Engle JW; Batista ER; Martin RL; Nortier FM; Fassbender ME; John KD; Birnbaum ER Evaluation of Nitrogen-Rich Macrocyclic Ligands for the Chelation of Therapeutic Bismuth Radioisotopes. Nucl. Med. Biol 2015, 42, 428–438. [PubMed: 25684650]

(99). Thiele NA; Woods JJ; Wilson JJ Implementing F-Block Metal Ions in Medicine: Tuning the Size Selectivity of Expanded Macrocycles. Inorg. Chem 2019, 58, 10483–10500. [PubMed: 31246017]

(100). Hu A; MacMillan SN; Wilson JJ Macrocyclic Ligands with an Unprecedented Size-Selectivity Pattern for the Lanthanide Ions. J. Am. Chem. Soc 2020, 142, 13500–13506. [PubMed: 32697907]

(101). Buist D; Williams NJ; Reibenspies JH; Hancock RD Control of Metal Ion Size-Based Selectivity through Chelate Ring Geometry. Metal Ion Complexing Properties of 2,2′-Biimidazole. Inorg. Chem 2010, 49, 5033–5039. [PubMed: 20446716]

(102). Cacheris WP; Nickle SK; Sherry AD Thermodynamic Study of Lanthanide Complexes of 1,4,7-Triazacyclononane-N,N',N"-Triacetic Acid and 1,4,7,10-Tetraazacyclododecane-N,N',N",N"'-Tetraacetic Acid. Inorg. Chem 1987, 26, 958–960.

(103). Cram DJ Preorganization—From Solvents to Spherands. Angew. Chem. Int. Ed 1986, 25, 1039–1057.

(104). Montavon G; Apostolidis C; Bruchertseifer F; Repinc U; Morgenstern A Spectroscopic Study of the Interaction of U(VI) with Transferrin and Albumin for Speciation of U(VI) under Blood Serum Conditions. J. Inorg. Biochem 2009, 103, 1609–1616. [PubMed: 19800129]

(105). Ansoborlo É; Amekraz B; Moulin C; Moulin V; Taran F; Bailly T; Burgada R; Hengé-Napoli MH; Jeanson A; Den Auwer C; Bonin L; Moisy P Review of Actinide Decorporation with Chelating Agents. Comptes Rendus Chim. 2007, 10, 1010–1019.

(106). Scapolan S; Ansorborlo E; Moulin C; Madic C Uranium (VI)-Transferrin System Studied by Time-Resolved Laser-Induced Fluorescence. Radiat. Prot. Dosimetry 1998, 79, 505–508.

(107). Ali M; Kumar A; Kumar M; Pandey BN The Interaction of Human Serum Albumin with Selected Lanthanide and Actinide Ions: Binding Affinities, Protein Unfolding and Conformational Changes. Biochimie 2016, 123, 117–129. [PubMed: 26821345]

(108). Kathren RL; Burklin RK Acute Chemical Toxicity of Uranium. Health Phys. 2008, 94, 170–179. [PubMed: 18188051]

(109). Yantasee W; Sangvanich T; Creim JA; Pattamakomsan K; Wiacek RJ; Fryxell GE; Addleman RS; Timchalk C Functional Sorbents for Selective Capture of Plutonium, Americium, Uranium, and Thorium in Blood. Health Phys. 2010, 99, 413–419. [PubMed: 20699706]

(110). Bergeron RJ; Wiegand J; Singh S Desferrithiocin Analogue Uranium Decorporation Agents. Int. J. Radiat. Biol 2009, 85, 348–361. [PubMed: 19399680]

(111). Paquet F; Houpert P; Blanchardon E; Delissen O; Maubert C; Dhieux B; Moreels AM; Frelon S; Voisin P; Gourmelon P Accumulation and Distribution of Uranium in Rats After Chronic Exposure by Ingestion. Health Phys. 2006, 90, 139–147. [PubMed: 16404171]

(112). Walinder G; Hammarström L; Billaudelle U Incorporation of Uranium: I. Distribution of Intravenously and Intraperitoneally Injected Uranium. Br. J. Ind. Med 1967, 24, 305–312. [PubMed: 6073089]

(113). Bolt AM; Medina S; Lauer FT; Xu H; Ali A-M; Liu KJ; Burchiel SW Minimal Uranium Accumulation in Lymphoid Tissues Following an Oral 60-Day Uranyl Acetate Exposure in Male and Female C57BL/6J Mice. PLoS One 2018, 13, e0205211. [PubMed: 30356336]

(114). Jim V; LaViolette C; Briehl MM; Ingram JC Spatial Distribution of Uranium in Mice Kidneys Detected by Laser Ablation Inductively Coupled Plasma Mass Spectrometry. J. Appl. Bioanal 2017, 3, 43–48. [PubMed: 29177200]

(115). Neuman WF; Fleming RW; Dounce AL; Carlson AB; O'Leary J; Mulryan B The Distrubution Excretion of Injected Uranium. J. Biol. Chem 1948, 173, 737–748. [PubMed: 18910729]

(116). Abou DS; Thiele NA; Gutsche NT; Villmer A; Zhang H; Woods JJ; Baidoo KE; Escorcia FE; Wilson JJ; Thorek DLJ Towards the Stable Chelation of Radium for Biomedical Applications with an 18-Membered Macrocyclic Ligand. Chem. Sci 2021, 12, 3733–3742. [PubMed: 34163647]

(117). Henriksen G; Fisher DR; Roeske JC; Øyvind; Bruland S; Larsen RH Targeting of Osseous Sites With-Emitting ^{223}Ra: Comparison with the-Emitter ^{89}Sr in Mice. J. Nucl. Med 2003, 44, 252–259. [PubMed: 12571218]

(118). Walinder G; Fries B; Billaudelle U Incorporation of Uranium. II. Distribution of Uranium Absorbed Through the Lungs and the Skin. Br. J. Ind. Med 1967, 24, 313–319. [PubMed: 6073090]

Synopsis:

The exploration of four acyclic hexadentate ligands as chelators for the uranyl ion for application in uranium-230 targeted alpha therapy is reported. The uranyl complexes were thoroughly characterized and were found to be stable when challenged with biologically relevant species in vitro over 14 days and remained intact in vivo. This is the first report of ligands that form complexes with the uranyl ion with excellent long-term stability under biologically relevant conditions.

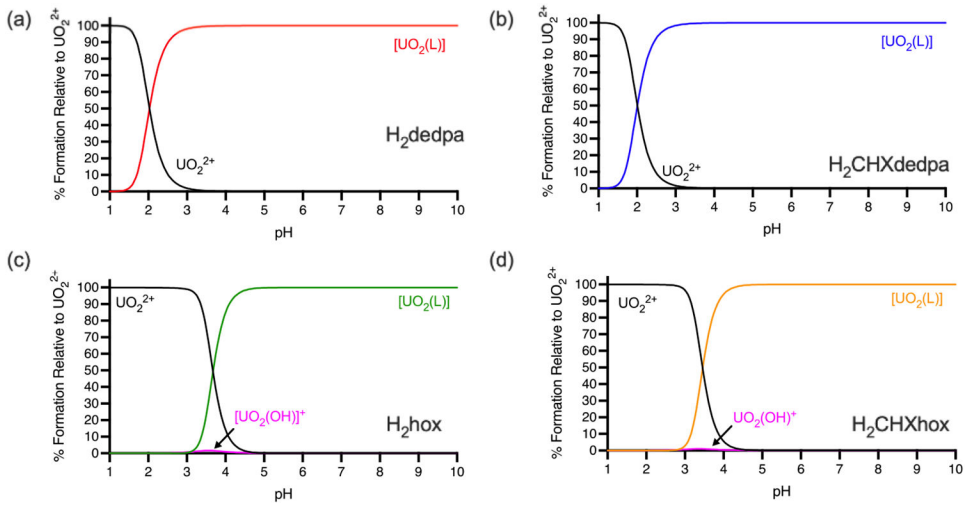

Figure 1.

Species distribution diagrams for (a) H_2dedpa, (b) H_2CHXdedpa, (c) H_2hox, and (d) H_2CHXhox in the presence of UO_2^{2+} at $[L]_{tot} = [UO_2^{2+}]_{tot}$ = 10 μM, I = 0.1 M KCl, 25 °C.

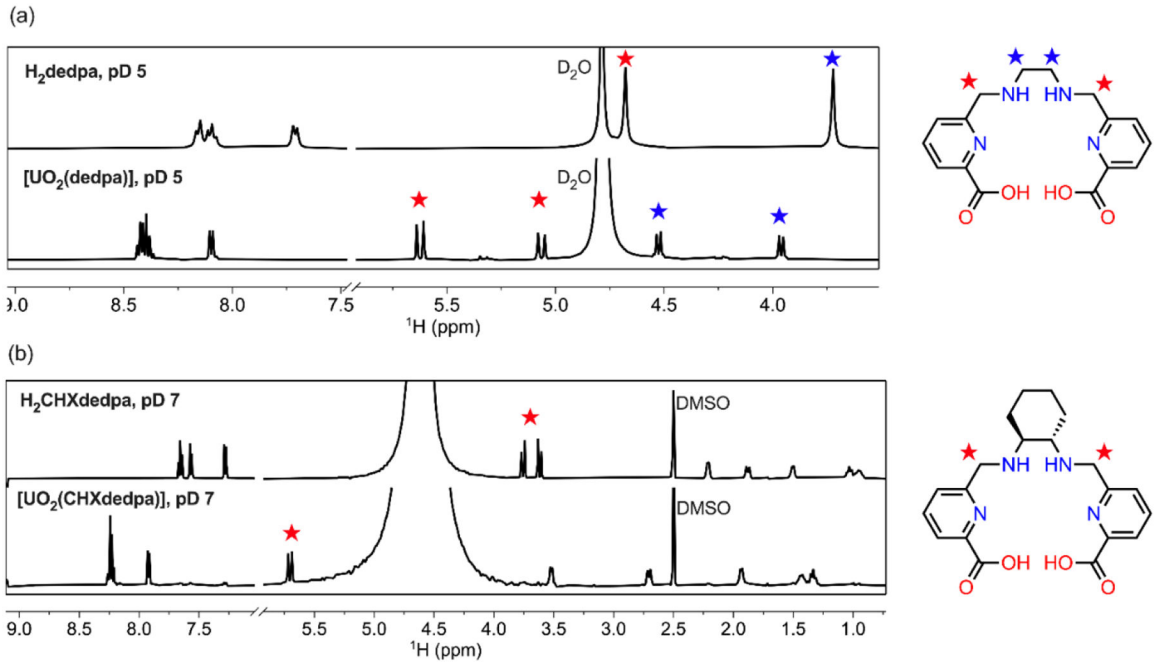

Figure 2.

Comparison of ^{1}H NMR (500 MHz, 25 °C) spectra of (a) H_2dedpa and [UO_2dedpa] in D_2O + 0.1% acetone at pD 5 and (b) H_2CHXdedpa and UO_2CHXdedpa in D_2O + 0.1% DMSO-d_6 at pD 7. The resonance corresponding to the second set of methylene protons of [UO_2(CHXdedpa)] is located under the D_2O peak.

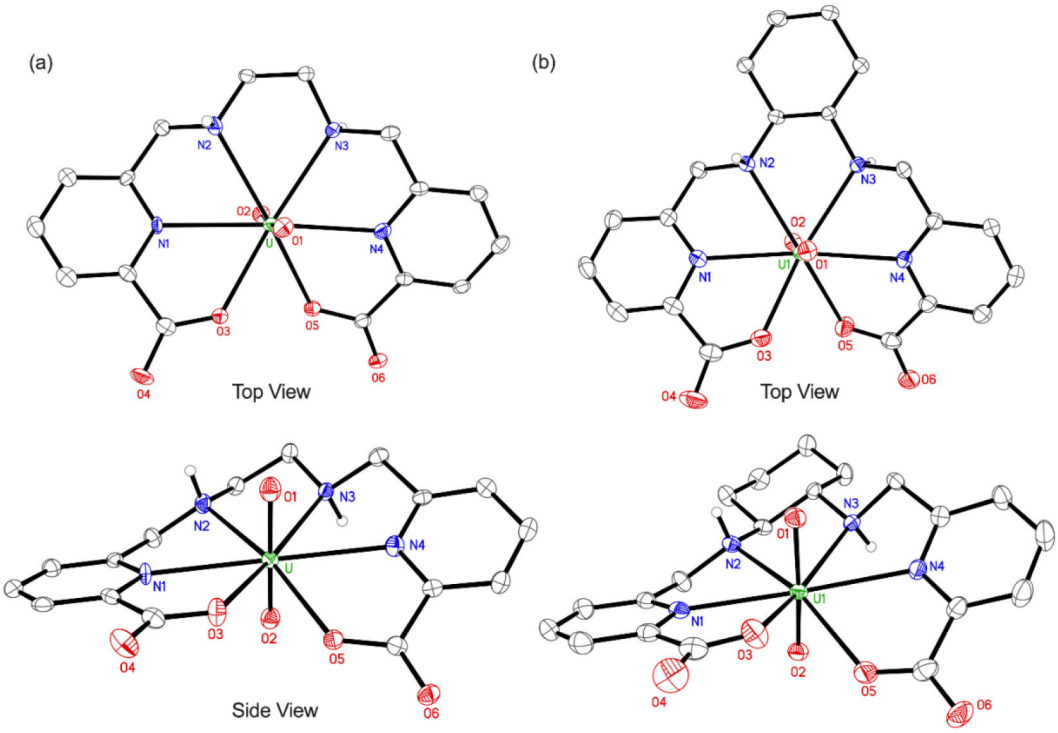

Figure 3.

X-ray crystal structures of (a) [UO_2(dedpa)] and (b) [UO_2(CHXdedpa)]. Thermal ellipsoids are drawn at the 50% probability level. Counterions, outer-sphere solvent molecules, and hydrogen atoms bound to carbon atoms are omitted for clarity. For [UO_2(CHXdedpa)], only one of the two independent molecules present in the asymmetric unit is shown.

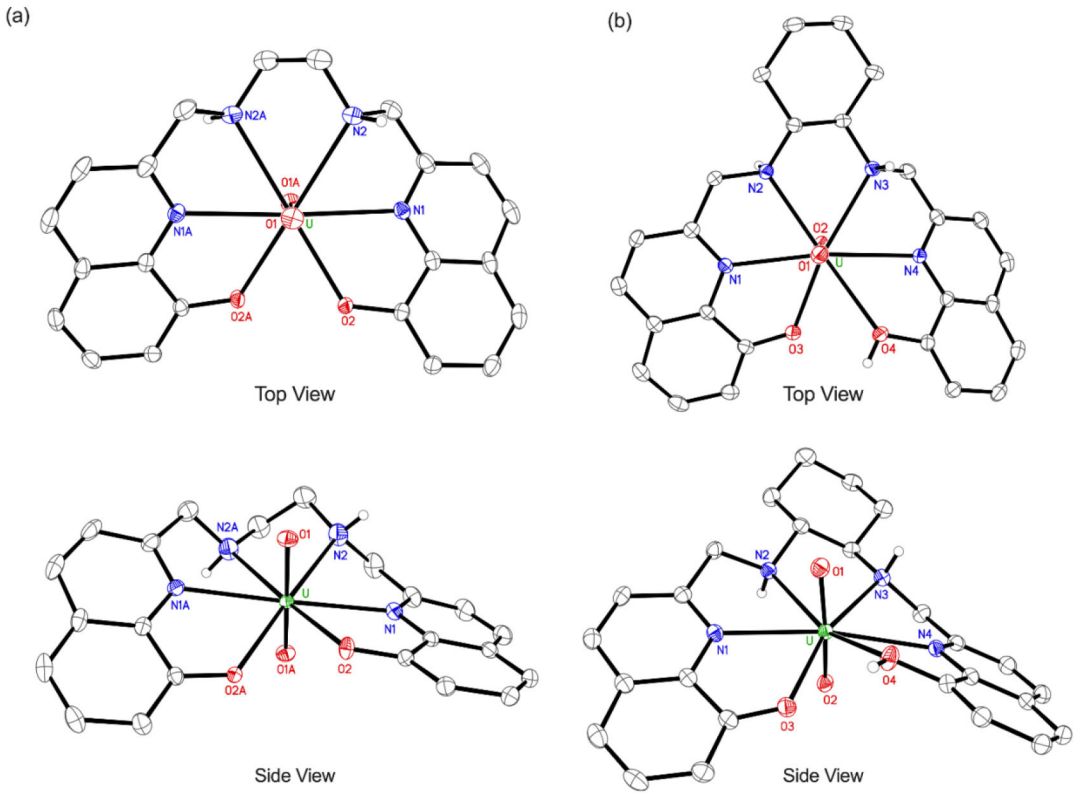

Figure 4.

X-ray crystal structures of (a) $[UO_2(hox)]$ and (b) $[UO_2(HCHXhox)](NO_3)$. Thermal ellipsoids are drawn at the 50% probability level. Counterions, outer-sphere solvent molecules, and hydrogen atoms bound to carbon atoms are omitted for clarity.

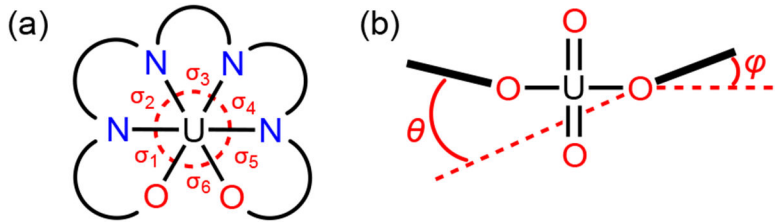

Figure 5.

Conformational metrics used to compare the relative ligand distortion in the X-ray crystal structures discussed here.

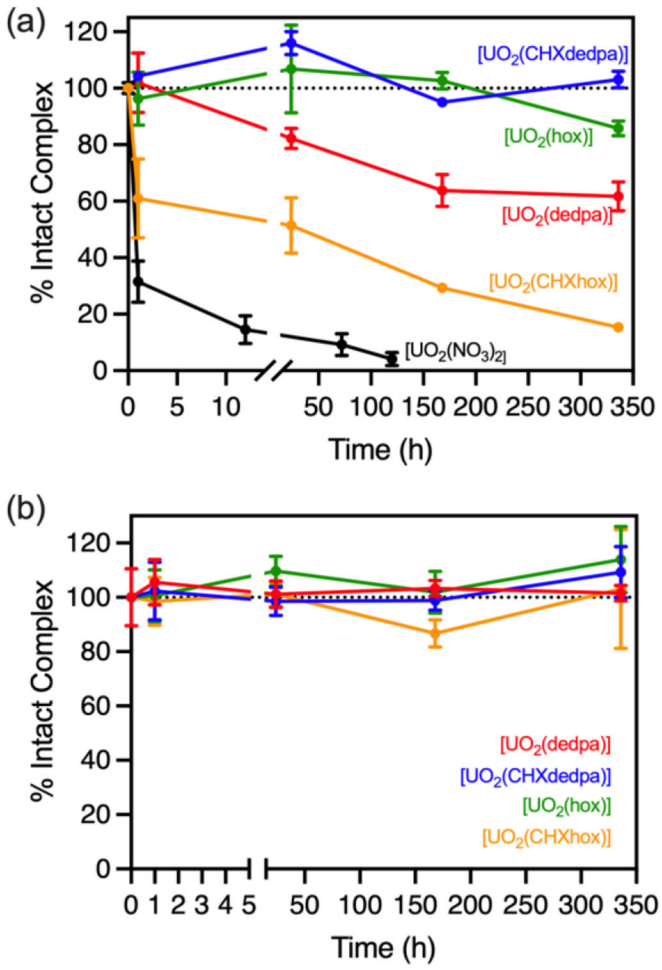

Figure 6.

Kinetic stability of [UO_2(L)] complexes in 0.1 M TRIS buffer (pH 7.4, 37 °C) containing (a) 2000 eq. HAP or (b) human plasma over 14 d as measured by HPLC.

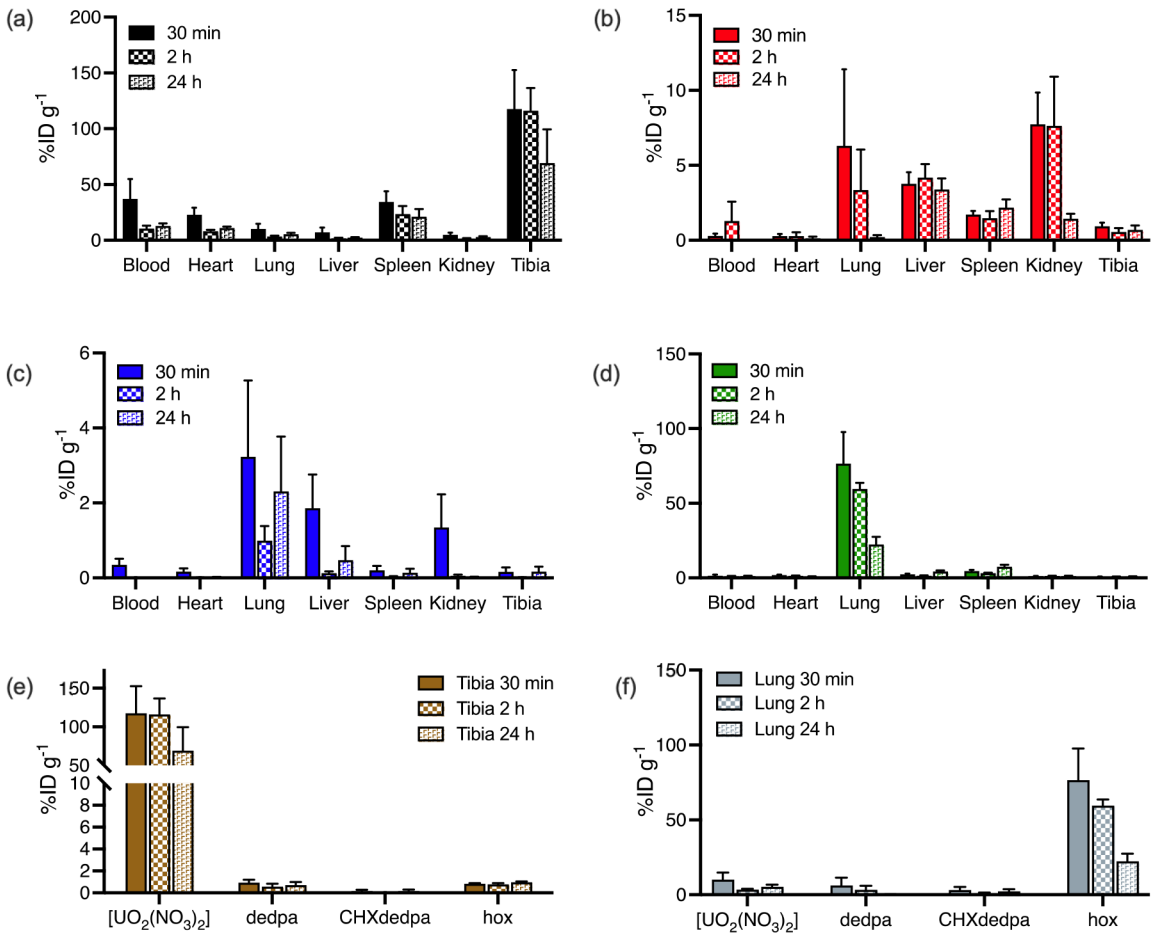

Figure 7.

Ex vivo biodistribution profiles of (a) $[UO_2(NO_3)]\cdot 6H_2O$, (b) $[UO_2(dedpa)]$, (c) $[UO_2(CHXdedpa)]$ and (d) $[UO_2(hox)]$ at 30 min, 2 h and 24 h. (e,f) Comparison of the uranium content in the (e) tibia and (f) lung for the data shown in a–d. Values are expressed as % initial dose per gram of tissue weight ± standard error of measurement (SEM; $n = 3–5$). Note the different scales of the y-axis of each panel.

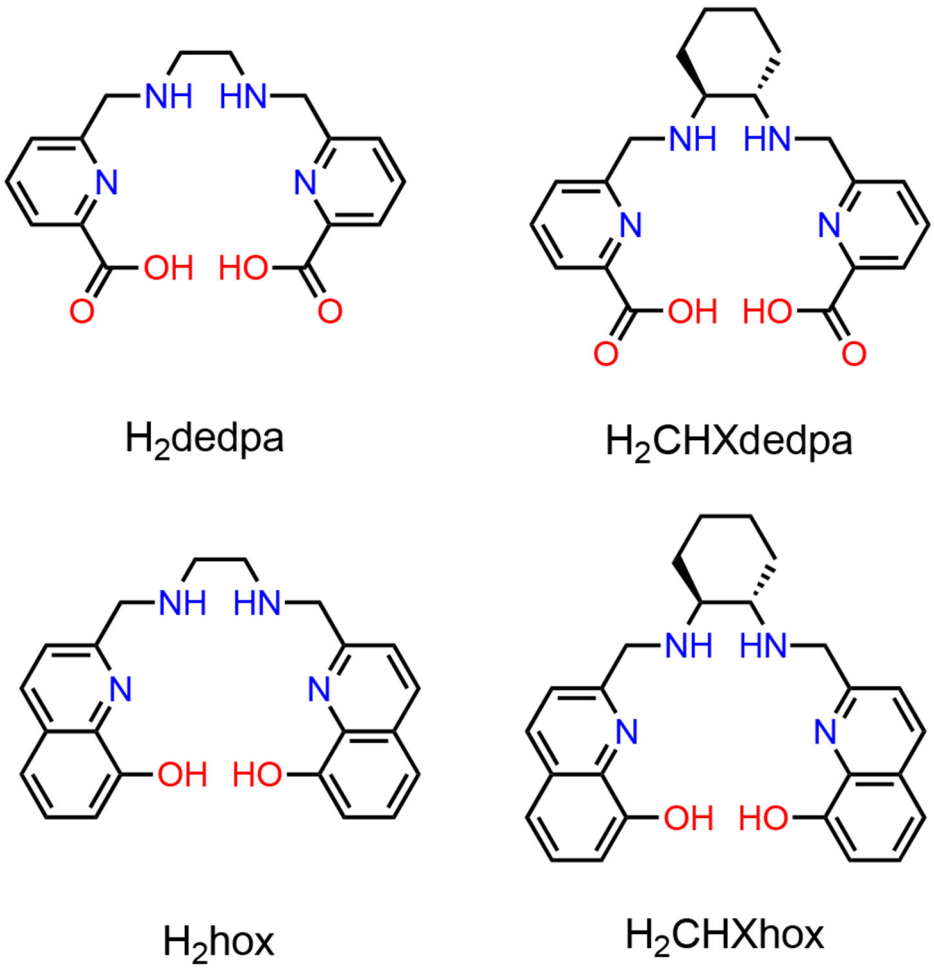

Chart 1.
Structures of Ligands Explored in this Study.

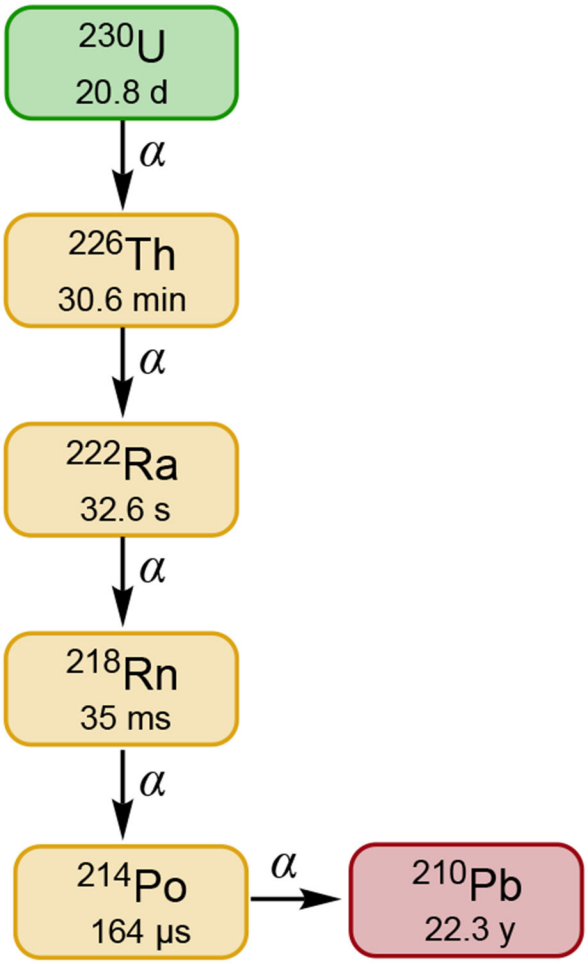

Scheme 1.
Decay Scheme of ^{230}U

Table 1.

Protonation Constants of H_2dedpa, H_2CHXdedpa, H_2hox, and H_2CHXhox and the Predicted and Experimental Thermodynamic Stability Constants of their UO_2^{2+} Complexes (25 °C, I = 0.1 M KCl).[a]

	H_2dedpa[b]	H_2CHXdedpa[b]	H_2hox[c]	H_2CHXhox[c]
pK_{a1}	8.95(3)	9.39(2)	11.0(1)	10.95(9)
pK_{a2}	6.32(6)	6.43(6)	10.10(8)	10.18(2)
pK_{a3}	3.15(6)	3.15(6)	8.63(5)	8.72(7)
pK_{a4}	2.28(7)	2.40(8)	6.1(3)	5.37(2)
Calc'd logβ_{ML}[d]	17.2	19.5	25.3	26.85
Expt'l logβ_{ML}	18.1(2)	18.8(1)	26.43(7)	26.7(1)
pUO_2 (pH 7.4)[e]	17.46	17.72	19.80	19.98

[a] The number given in parentheses corresponds to the standard deviation of the last digit of the stability constant.

[b] Determined by potentiometric titration, 25 °C, I = 0.1 M.

[c] Determined by spectrophotometric titration, 25 °C, I = 0.1 M.

[d] Predicted using the regression equation given Figure S54, 25 °C, I = 0 M.

[e] $pUO_2 = -\log[UO_2^{2+}]_{free}$ ($[UO_2^{2+}]_{tot} = 10^{-6}$ M; $[L]_{tot} = 10^{-5}$ M; pH 7.4; 25 °C; I = 0.1 M KCl).

Table 2.

Second-Order Rate Constants (k_2, M^{-1} s^{-1}) and Half-Lives ($t_{1/2}$, s) for the Complexation of UO_2^{2+} by the Ligands at 25 °C in Aqueous Solution.

Ligand	k_2 (pH 5)	k_2 (pH 7.4)	$t_{1/2}$ (pH 5)[a]	$t_{1/2}$ (pH 7.4)[a]
dedpa	420 ± 28	450 ± 40	240	220
CHXdedpa	1320 ± 140	1190 ± 150	76	84
hox	73 ± 5	3420 ± 340	1370	29
CHXhox	140 ± 5	2850 ± 380	714	35

[a] calculated using 10 μM ligand + 10 μM UO_2^{2+}

Table 3.

Selected Interatomic Distances (Å) and Angles (°) for the Structures of the UO_2^{2+} Complexes.

Complex	O_{yl}–U–O_{yl}	U–O_{yl}	U–$O_{pic/ox}$	U–$N_{pyr/ox}$	U–N_{am}
[(UO_2)dedpa]	173.3(2)	1.770(6), 1.776(5)	2.403(3), 2.454(6)	2.650(7), 2.643(5)	2.653(9), 2.652(9)
[(UO_2)CHXdedpa][b]	168.90(9); 170.30(9)	1.795(2), 1.781(2); 1.777(2), 1.794(2)	2.386(2), 2.439(2); 2.412(2), 2.420(2)	2.599(2), 2.602(2); 2.588(2), 2.607(2)	2.633(2), 2.642(2); 2.619(2), 2.644(2)
[(UO_2)hox][c]	172.84(15)	1.784(2)	2.405(2)	2.608(2)	2.651(3)
[(UO_2)HCHXhox]$^+$	169.89(9)	1.779(2), 1.791(2)	2.300(2), 2.638(2)	2.558(3), 2.621(3)	2.607(2), 2.625(2)

[a] O_{pic} = picolinate oxygen, O_{ox} = oxine oxygen, N_{pyr} = picolinate oxygen, N_{quin} = oxine nitrogen, N_{am} = amine nitrogen.

[b] There are two independent molecules in the asymmetric unit.

[c] The complex sits on a crystallographic C_2 axis, such that the asymmetric unit consists of one half of the molecule.

Table 4.

Conformational Metrics Used to Evaluate the Structures of $[UO_2(H_nL)]^{m+}$ ($m = 0$, $n = 0$; $m=1$, $n = 1$) Complexes.

Ligand	σ_1 (°)	σ_2 (°)	σ_3 (°)	σ_4 (°)	σ_5 (°)	σ_6 (°)	$\Sigma\sigma_n$ (°)	θ (°)	φ (°)
dedpa	60.3(2)	60.5(2)	63.1(2)	59.9(2)	61.3(2)	62.4(2)	367.5	38.35	19.00, 20.40
CHXdedpa[a]	61.90(8); 61.96(7)	61.82(7); 62.22(7)	64.06(7); 64.17(7)	60.59(7); 60.05(7)	61.48(8); 61.35(7)	65.17(8); 64.87(7)	375.02; 374.62	42.91; 52.96	18.83, 27.67; 21.68, 33.89
hox	62.55(8)	58.83(9)	62.76(13)	58.83(9)	62.55(8)	65.15(11)	370.6	35.49	20.61, 20.61
CHXhox	64.49(7)	62.07(7)	64.75(7)	61.13(7)	59.26(7)	64.10(7)	375.8	41.65	19.37, 30.70

[a]There are two independent molecules in the asymmetric unit

Table 5.

Strain Energies (ΔG_S, kcal mol^{-1})[a] of Ligands in their UO_2^{2+} Complexes.

Ligand	ΔG_s (kcal mol^{-1})[a]
H_2dedpa	40.5
H_2CHXdedpa	34.8
H_2hox	11.4
H_2CHXhox	0

[a] normalized to H_2CHXhox, which displays the lowest ΔG_S